A novel approach to estimation of residual strength of laminated polymer composites under compression after impact

Oleg Staroverov, Anastasia Sivtseva, Artur Mugatarov, Sevastyan Koksharov
Perm National Research Polytechnic University, Russia
cem_staroverov@mail.ru, oastaroverov@pstu.ru, https://orcid.org/0000-0001-6095-0962
cem_sivtseva@mail.ru, https://orcid.org/0000-0002-4348-7491
cem_mugatarov@mail.ru, https://orcid.org/0000-0002-2229-8181
Kosevfun@gmail.com, https://orcid.org/0009-0000-8020-6882

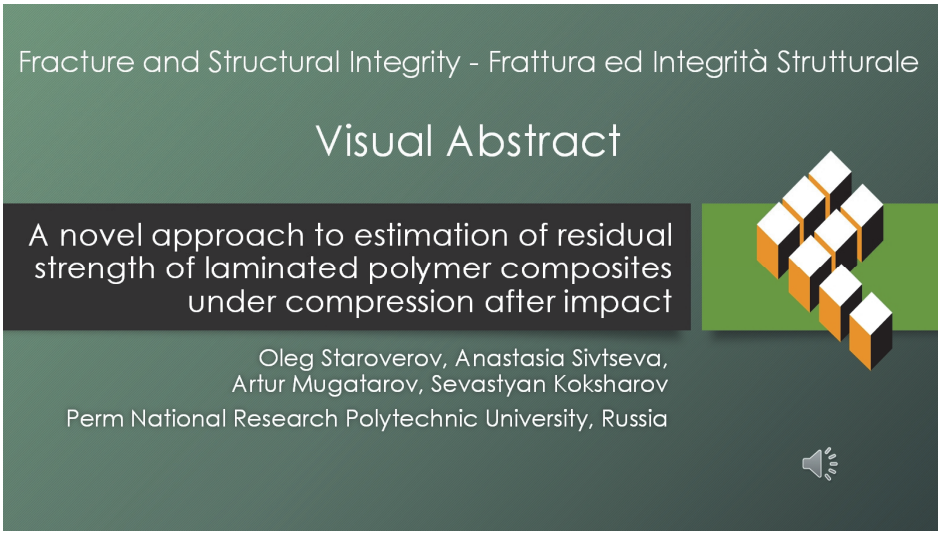

Citation: Staroverov, O., Sivtseva, A., Mugatarov, A., Koksharov, S., A novel approach to estimation of residual strength of laminated polymer composites under compression after impact, Fracture and Structural Integrity, xx (2025) ww-zz.

Received: 15.08.2025
Accepted: 10.09.2025
Published: 11.09.2025
Issue: 10.2025

KEYWORDS. Polymer composites, Low-velocity impact, Compression after impact, Residual mechanical characteristics, Impact sensitivity, Ultrasonic testing.

INTRODUCTION

Polymer composite materials reinforced with long fibers are widely used in high-load units and facilities of civil aviation, shipbuilding, automotive, etc., due to their light specific weight and high physical and mechanical properties. When modelling composite structures, it is necessary to consider the conditions of their operation, especially in the case of operation under the influence of cyclic or impact loadings, which can lead to the accumulation of structural damage and a change in mechanical behavior at the macro level. Consideration of the influence of impacts is especially important when designing structures from laminated composites due to their low strength when deformed across the direction of lamination (for example, in cases of indentation, transverse impact, or explosive loadings) [1, 2].
Studies of polymer composites' resistance are carried out for cases of both high-velocity [3, 4] and low-velocity [5–7] impacts. As a result of low-velocity impact, mixed fracture mechanisms realize (matrix cracking, delamination, fiber breaks), at the

same time, damage arising in the structure may not be visible to the naked eye (especially when using carbon fiber), but affect the residual mechanical properties. Most often, researchers study the influence of preliminary low-velocity impact on the mechanical properties of composites under compression [8–11], but studies of residual properties under tension [12–15], bending [16, 17] and shear [18] can also be noted. In addition to the energy and impact velocity influence, the authors considered issues related to the variation in the size and thickness of specimens [16, 17, 19, 20], reinforcement scheme [21], and the shape of the impactor [11, 16]. The authors [8, 12, 13] note the presence of a threshold for strength properties sensitivity to impacts with low energy.

Earlier, the authors [22] proposed an approach to predicting the residual properties of polymer composites, based on the construction of impact sensitivity diagram – the dependence of the residual static strength (bearing capacity) on the impact energy. In these diagrams, it seems expedient to determine two characteristic threshold values of the impact energy: the first corresponds to the end of the area, in which the impact nearly does not affect the residual properties, the second – to the beginning of the area, in which an increase in the impact energy almost does not lead to a change in the material's strength, since the damaged composite reaches its minimum strength. To determine these threshold values, it is necessary to create mathematical models for describing experimental dependences of the residual strength on impact energy. Some researchers used power [22, 23] and exponential [24] functions to approximate experimental data.

The aim of this work is to further develop the previously proposed approach for assessing the influence of preliminary low-velocity local impacts of various energies on the residual strength under compression and to develop principles for determining threshold values of impact sensitivity based on the construction of mathematical models for describing experimental dependencies.

MATERIAL AND METHODS

Experimental studies were carried out using Unique Scientific Equipment "A complex of testing and diagnostic equipment to study the properties of structural and functional materials under complex thermomechanical loading conditions" (http://ckp-rf.ru/usu/501309/).

Structural glass fiber polymer composite VFT-S (GFRP), provided by Ural-Izolit LLC (Russia, Yekaterinburg) and manufactured in accordance with GOST 10292-74, was chosen as the material for the study. The specimens had dimensions of 150 × 100 × 3 mm and were cut from one plate along the fibers and at an angle of 45° to the fibers, which corresponds to the reinforcement schemes $[0/90]_n$ and $[\pm 45]_n$. The experimental part of the study included the following steps:

1. Quasi-static compression of specimens without preliminary low-velocity impact in order to determine the maximum load P_{max} and ultimate strength (bearing capacity) F_0^{CAI} (ASTM D7137). The tests were carried out on the Instron 5882 universal electromechanical test system (Fig. 1a) with a maximum tensile/compressive load of ± 100 kN and a load cell accuracy of 0.5 %. The traverse speed was 1.3 mm/min. To prevent buckling during compression, the specimens were installed into the special device (Fig. 1b).
2. Preliminary low-velocity impact with different energy E_{imp} (ASTM D7136). Tests were carried out on the Instron CEAST 9350 electrodynamic system (Fig. 1c, 1d), which allows to perform impacts with energy in the range from 0.7 to 1800 J. In this study, single transverse (relative to the direction of the reinforcement layers) impacts were applied with a hemispherical tip with the diameter of 16 mm; the total mass of the drop system, the height and velocity of impact for each energy level are presented in Tab. 1. For the study, 10 levels of impact energy were selected in the range of 10–100 J, at each of which 3 specimens were tested.
3. An ultrasonic flaw detector TD FOCUS-SCAN RX, a 64-element linear phased array PA-W40-5L64 with an operating frequency of 5 MHz and a combined piezoelectric transducer DL5P6 with an acoustic delay line made of polystyrene and an operating frequency of 5 MHz were used to assess the lamination area S formed as a result of low-velocity drop-weight impact. NDTest acoustic gel was used as the contact fluid. Results were processed by using TD-Scan software. Due to the fact that during high-intensity impacts there is breakthrough that prevents the installation of detectors on two opposite sides of the specimen, an echo-pulsed technique of ultrasonic testing was used, which allows one-side scanning. 8 piezoelectric elements were active during testing with the phased array, the focal point was set at a depth of 2 mm from the controlled surface. The delamination boundaries were determined by the decrease in the amplitude of the once reflected bottom echo signal from 80 to 40%. The delamination area was calculated by using the CarlZeiss SteREO Discovery V12 optical stereo microscope and the ZEN software. The study of the physical processes occurring in the structure of composites under complex impact and quasi-static effects, based on data obtained by using the method of ultrasonic scanning and optical microscopy, was carried out as part of the University Development Program for 2025-2036 with the support of the Strategic Academic Leadership Program "Priority-2030," Agreement No. 075-15-2025-216 of 04.04.2025.

4. Quasi-static compression of specimens after impact (performed under conditions similar to those described in step 1) with determination of residual strength F^{CAI} (ASTM D7137).

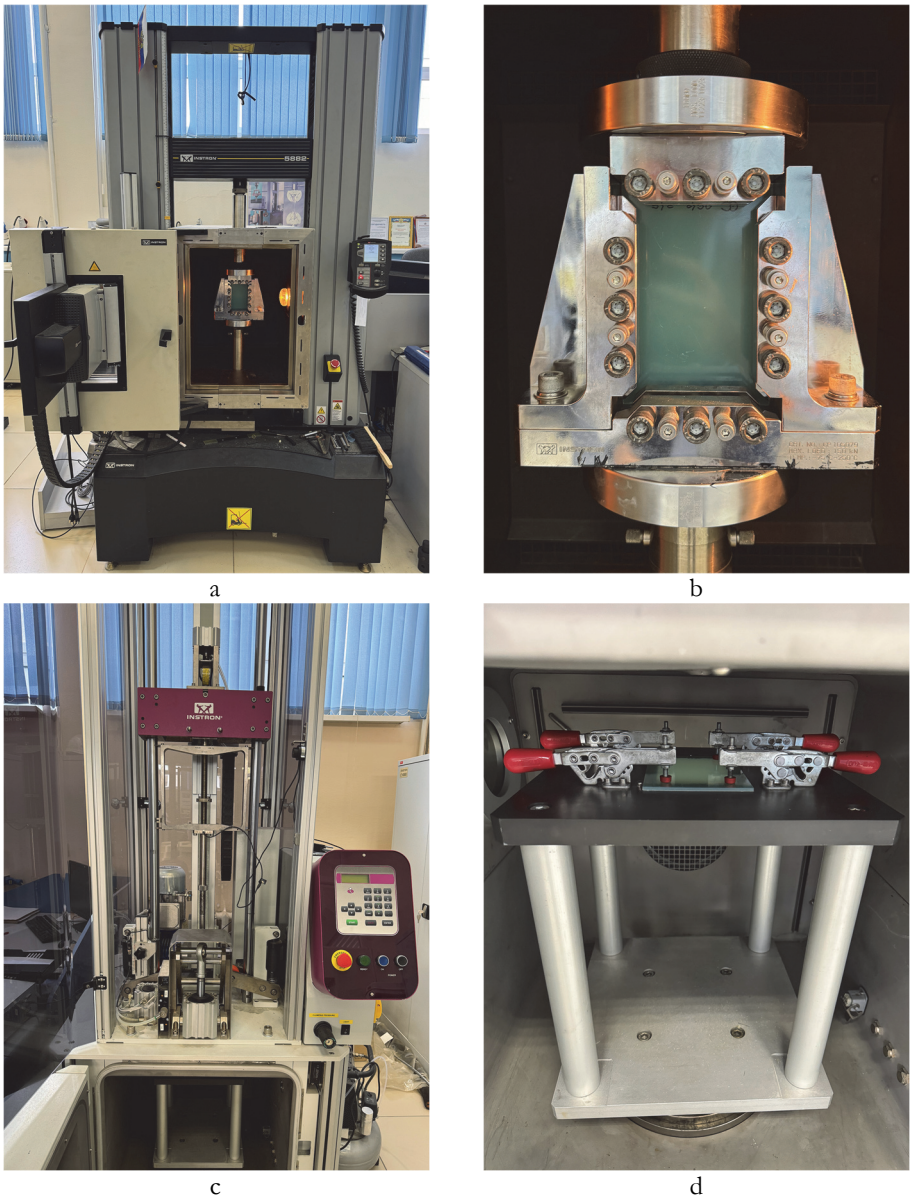

Figure 1: Test systems: Instron 5882 system (a), specimen in the device preventing buckling during compression (b), Instron CEAST 9350 system (c), specimen in the support stand with clamping devices for impact testing (d)

Parameter	Impact energy E_{imp}, J									
	10	15	20	30	35	40	50	60	75	100
Weight, kg	5.048	5.048	5.048	5.048	5.048	5.048	10.048	10.048	10.048	15.048
Velocity, m/s	1.99	2.44	2.84	3.45	3.72	3.98	3.15	3.46	3.86	3.65
Height, m	0.202	0.303	0.411	0.607	0.705	0.808	0.506	0.610	0.760	0.679

Table 1: Impact parameters

RESULTS AND DISCUSSION

Drop-weight impact tests with controlled parameters

Based on the results of impact tests with different energy, typical dependencies of contact load on displacement (Fig. 2a, 2b), load on time (Fig. 2c, 2d), energy on time (Fig. 3a, 3b) were plotted for specimens with reinforcement schemes $[0/90]_n$ and $[\pm45]_n$. Average values of peak load, absorbed energy, maximum and residual displacement are shown in Tab. 2.

In the impact energy range of 10–20 J, on the diagram of load dependency on displacement (Fig. 2a, 2b) pronounced stages of linear and nonlinear load growth and smooth unloading are shown. Small areas of "plateau" on the diagrams "load–time" (Fig. 2c, 2d) may correspond to the process of energy absorption by specimens, due to the matrix cracking in the upper layers of the material and the beginning of delamination. When the impact energy increases to 30–50 J, the essence of the diagrams changes, a sharp drop in load is noted after reaching the peak, which corresponds to the energy consumption for delamination and breaking of fibers on the surface area that directly contacts the impactor. In the case where the impact energy was 60–100 J, there was a repeated increase in load after reaching the minimum point. This effect is explained by the breaking through the specimen, after which further braking of the impactor occurs mainly due to deformation and secondary contact with already damaged parts of the specimen (they break with the fracture of the matrix). It is also noted that as the impact energy increases, the maximum displacement and impact time increases. The non-monotonic change of the residual displacement value might be connected with the oscillation of the specimen after the impact.

It was discovered that the found patterns are equivalent for specimens cut along the direction of the fibers and at an angle of 45° to them. However, for specimens with reinforcement scheme $[\pm45]_n$, the peak loads occurring during impact were higher than for specimens with stacking sequence $[0/90]_n$. This phenomenon may be due to the fact that the total length of the fibers, providing primary resistance to the impactor, differs for two reinforcement schemes: with the $[0/90]_n$ scheme, it is proportional to the sum of the length and width of the specimen (≈ 250 mm), while with the $[\pm45]_n$ scheme it is proportional to twice the diagonal of the square with a width of 100 mm, which is ≈ 283 mm. An increase in this value corresponds well to an increase in load by about 8–22 % (depending on the energy level).

From the graphs of energy growth over time (Fig. 3), it can be seen that in the range of 10–40 J, the energy absorbed by the specimen is less than the initial impact energy, which occurs due to the accumulation of damage (matrix cracking, delamination, fiber breaks), the remaining energy corresponds to the kinetic energy of the impactor after bouncing off of the specimen's surface. At high impact energy levels (50–100 J), a monotonous increase in absorbed energy values is observed, which indicates a breakthrough of the specimen. In this case, in order to determine the absorbed energy spent on fracture of the structural elements before breaking, it is necessary to take into account the previously noted effect of braking the impactor due to deformation of already damaged parts of the specimen, and to determine the absorbed energy at a point corresponding to the minimum load (two energy growth areas are clearly visible on the graphs). The values of absorbed energy calculated in this way are presented in Tab. 2. The obtained data confirm that the breakthrough energy is about 50 J.

	Average value of impact parameter	Impact energy E_{imp}, J									
		10	15	20	30	35	40	50	60	75	100
GFRP $[0/90]_n$	Peak load, kN	3.3	4.0	3.4	4.9	4.4	4.7	4.7	4.2	4.9	4.6
	Absorbed energy, J	7.7	9.9	19.8	23.1	33.3	38.3	47.8	47.4	50.6	49.4
	Maximum displacement, mm	4.6	5.8	8.4	8.9	11.6	12.5		breakthrough		
	Residual displacement, mm	2.3	1.9	7.6	4.2	10.1	11.1		breakthrough		
GFRP $[\pm45]_n$	Peak load, kN	3.3	4.5	4.1	5.6	5.2	5.3	5.4	5.1	5.8	4.9
	Absorbed energy, J	6.6	5.6	17.5	25.2	34.0	33.1	46.9	47.9	47.6	40.9
	Maximum displacement, mm	4.6	5.6	7.5	8.7	11.0	11.3		breakthrough		
	Residual displacement, mm	1.6	0.0	4.8	4.8	9.6	10.0		breakthrough		

Table 2: Average values of peak load, absorbed energy, maximum and residual displacement

The results of visual inspection of impacted specimens (Fig. 4) confirm the patterns identified on the basis of the diagrams' analysis, obtained on the dynamic test system. It is noted that the type of damaged areas almost did not depend on the reinforcement scheme of the composite. At impact energies of 10–15 J, there is a slight increase in the area of the damaged zone *S* and cracking of the surface (i.e. local destruction of the matrix) with little delamination, with virtually no damage to the fibers, is observed. With a further increase in energy, up to 40 J, there is a gradual increase of the damage area, breakage of the fibers of the reinforcement system takes place, and the delamination zone gradually grows. With an impact energy of

50 J or more, a breakthrough of the specimens occurs; with the reinforcement scheme $[0/90]_n$, growth of the lamination area stops, while with the scheme $[\pm 45]_n$, it continues to increase to E_{imp} = 75 J.

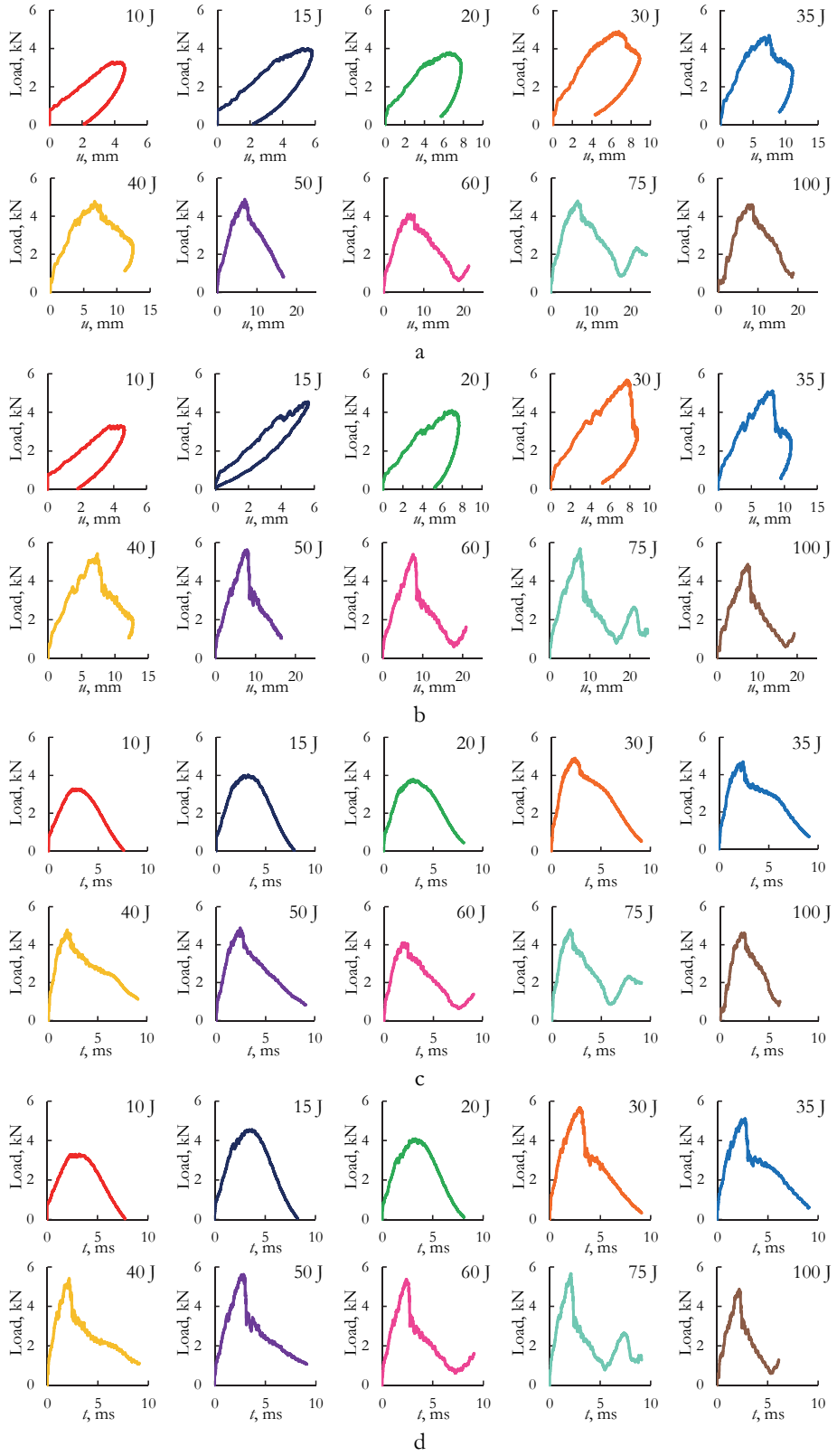

Figure 2: The dependences of load on displacement and load on time for specimens with reinforcement schemes $[0/90]_n$ (a, c) and $[\pm 45]_n$ (b, d), respectively

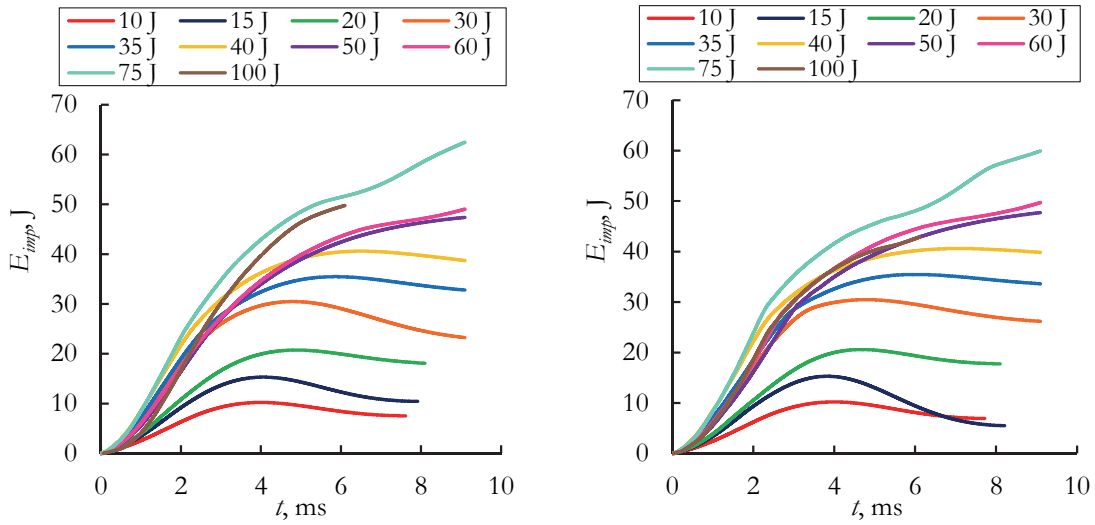

Figure 3: The dependences of energy on time for specimens with reinforcement schemes $[0/90]_n$ (a) and $[\pm 45]_n$ (b)

Figure 4: Images of specimens with the reinforcement schemes $[0/90]_n$ (a) and $[\pm 45]_n$ (b) after impacts

The dependence of the delamination area S, determined by using an ultrasonic flaw detector, on the impact energy E_{imp} was plotted (Fig. 5). It is noted that for the reinforcement scheme $[0/90]_n$, this dependence grows almost linearly to an impact energy of 50 J, after which it nearly does not change, reaching a value of about 1750 mm^2. For composite $[\pm45]_n$, the growth of the delamination area is almost linear in the range of impact energies of 10–75 J; for E_{imp} = 100 J, a decrease in the delamination area is observed, which is explained by an increase in the mass of the impactor. Since the residual strength of the composite under compression correlates with the delamination area [1, 8], it can be assumed that the energy threshold value, after which there is almost no further reduction in strength, will be about 50 J for fiberglass composite with reinforcement scheme $[0/90]_n$ and 75–100 J for composite $[\pm45]_n$.

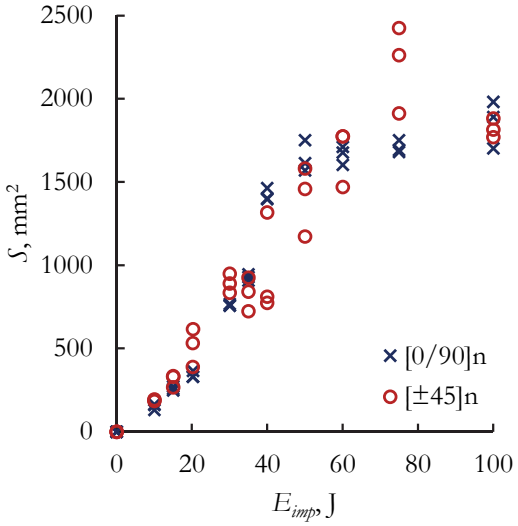

Figure 5: The change in the area of the delamination area depending on the impact energy

Compression after impact tests

After quasi-static compression testing of the specimens after the impact, loading diagrams were plotted, the typical form of which is shown in Fig. 6 (for better visualization of the results, the curves are offset 0.25 mm along the abscissa axis). It is noted that the qualitative type of loading diagrams does not depend on the energy of the preliminary impact: there is an initial section of non-monotonic deformation associated with the beginning of the movement of the test machine's parts and the loading device with the specimen; elastic deformation area with almost linear load growth; then nonlinear deformation of the specimens occurs, achieving maximum bearing capacity; after which the specimens with the structure $[0/90]_n$ have a sharp load drop, while the specimens with the reinforcement scheme $[\pm45]_n$ show a fairly stable postcritical deformation (load drop during growing displacement), followed by a drop. Tab. 3 shows the F^{CAI} residual strength values calculated from the compression tests.

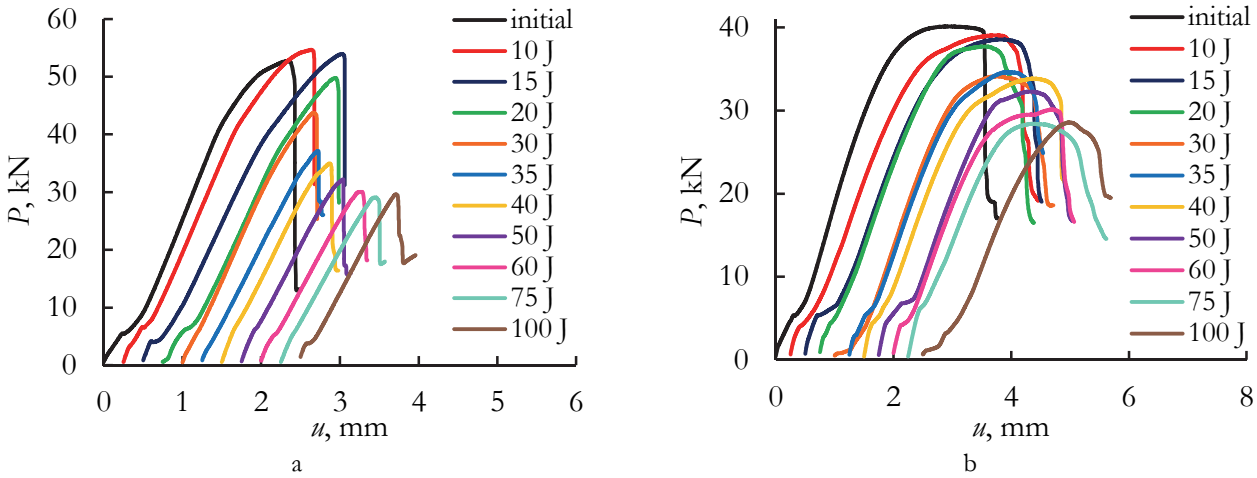

Figure 6: Loading diagrams of specimens with stacking sequence $[0/90]_n$ (a) and $[\pm45]_n$ (b) under quasi-static compression after impact

Specimen number	E_{imp}, J	GFRP $[0/90]_n$		GFRP $[\pm45]_n$	
		F^{CAI}, MPa	Average F^{CAI}, MPa	F^{CAI}, MPa	Average F^{CAI}, MPa
1	0	174		134	
2	0	176	175.7±1.5	129	131.3±2.5
3	0	177		131	
4	10	181		132	
5	10	180	178.7±3.2	134	132.0±2.0
6	10	175		130	
7	15	169		126	
8	15	181	176.3±6.4	124	126.7±3.1
9	15	179		130	
10	20	168		123	
11	20	164	165.7±2.1	125	124.3±1.2
12	20	165		125	
13	30	114		114	
14	30	136	129.7±13.7	114	115.3±2.3
15	30	139		118	
16	35	121		115	
17	35	122	124.3±4.9	115	115.0±0.0
18	35	130		115	
19	40	116		108	
20	40	103	112.3±8.1	115	113.3±4.7
21	40	118		117	
22	50	106		106	
23	50	102	104.0±2.0	108	107.0±1.0
24	50	104		107	
25	60	97		110	
26	60	95	97.0±2.0	96	102.0±7.2
27	60	99		100	
28	75	100		90	
29	75	96	99.0±2.6	116	100.3±13.8
30	75	101		95	
31	100	96		96	
32	100	98	97.3±1.2	92	95.7±3.5
33	100	98		99	

Table 3: Compression test results

Impact sensitivity diagrams in the form of F^{CAI} (E_{imp}) dependence (Fig. 7a) were plotted based on the test results. Three characteristic stages can be noted on the diagram of fiberglass composite's impact sensitivity: I – the area of insensitivity to impact (up to $E_{imp} \approx$ 15–20 J); II – the area of bearing capacity reduction – the most dangerous in terms of possible influence on the structure's strength; III – the area of reaching the minimum bearing capacity (experimental points form almost

horizontal section). Thus, the construction of impact sensitivity diagrams allows identifying two threshold values corresponding to transitions between stages.

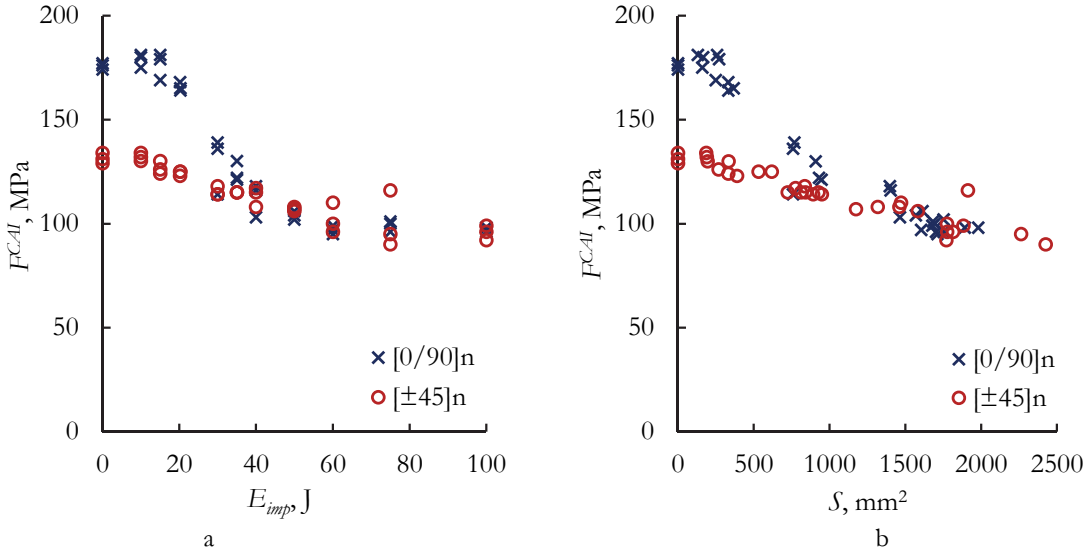

Figure 7: Residual strength of specimens under compression after impacts of different energies (a) and $F^{CAI}(S)$ dependence (b)

It was found that the considered GFRP has anisotropy in terms of sensitivity to low-velocity transverse impact: reduction in strength of the material with the reinforcement scheme $[0/90]_n$ is about 45 %, while for the scheme $[\pm45]_n$ the reduction is about ≈ 25 %. This peculiarity is explained by various mechanisms of composite's deformation during compression in different directions: when deforming along the fibers, the fibers bear the load, while when deforming at an angle of 45 ° to them, an in-plane shear and fibers rotation are realized, failure occurs in the plane oriented at an angle to the cross section. It is significant that the discovered pattern correlates with the results of the study of stress concentrators influence on the behavior of carbon fiber polymer composites with similar reinforcement schemes under tension [25]. It was noted that the F^{CAI} (E_{imp}) diagrams for two reinforcement schemes converge at energies of more than 50 J, i.e. at the breakthrough, but this effect may not be observed at other plate geometries and for other materials.

Fig. 7b shows the dependence of F^{CAI} composite's residual strength on the delamination area S. The results demonstrate the presence of a small area of insensitivity of the residual strength to the presence of impact-induced delamination (up to S = 200–250 mm²), then almost linear relationship of these parameters is observed (the correlation coefficient below –0.9 indicates a strong negative linear correlation). Accordingly, it can be concluded that the evaluation of the GFRP's residual strength after impact can be carried out on the basis of ultrasonic testing of damaged areas. It is advisable to build appropriate models, but this requires an additional study of the influence of the geometry, mass and impactor's velocity on the delamination area [11, 16].

The specimens were visually inspected after compression tests (Fig. 8). It is significant that with a minimum impact energy of 10 J, the failure of the specimen with the reinforcement scheme $[0/90]_n$ occurs outside the damaged area, which confirms the lack of material's sensitivity to impact in the range of 0–10 J. With an impact energy of 15 J, in some cases the failure occurred outside the impact zone, in some – in the area of the impact. Accordingly, it can be assumed that an energy value of about 15 J is close to the threshold of the impact insensitivity stage. A further increase in energy led to an increase in macrocrack from the damaged area orthogonal to the direction of load application. For specimens $[\pm45]_n$, failure in all cases occurred through the damaged area, however, the macrodefect had a complex shape, in some cases its branching was observed in accordance with the direction of the reinforcing fibers. This confirms the implementation of in-plane shear when compressing the composite at an angle of 45° to the direction of the fibers.

Novel approach to the analysis of the dependence of residual strength on impact energy based on mathematical models

As demonstrated above, the experimental dependence of GFRP's residual strength on the impact energy have three characteristic stages: I – a slight impact influence on strength; II – strength reduction at impact energy increase; III – reaching of minimum bearing capacity, when an increase in impact energy does not lead to a decrease in strength. Requirements for continuous functions that can be used to approximate experimental dependencies should be defined. Firstly, this function should be non-growing – it is assumed that the application of impact damage cannot increase the structure's strength. The

fulfillment of this condition corresponds to the non-positive value of the derivative of the approximation function (with exception of points, at which the derivative may not exist – when $E_{imp} = 0$, as well as when using piecewise-defined functions). Secondly, this function must satisfy the condition $F^{CAI}\left(E_{imp} = 0\right) = F_0^{CAI}$ – strength of the intact plate. Thirdly, this function should be limited from bellow by the line $F^{CAI} = F_{crit}^{CAI}$ – the value of the minimum bearing capacity. Fourthly, since there are three characteristic stages of damage accumulation "slow"–"fast"–"slow," and the dependence of the residual strength on the impact energy is non-monotonic, the selected function must have one inflection point or a critical point (when using a piecewise-defined function).

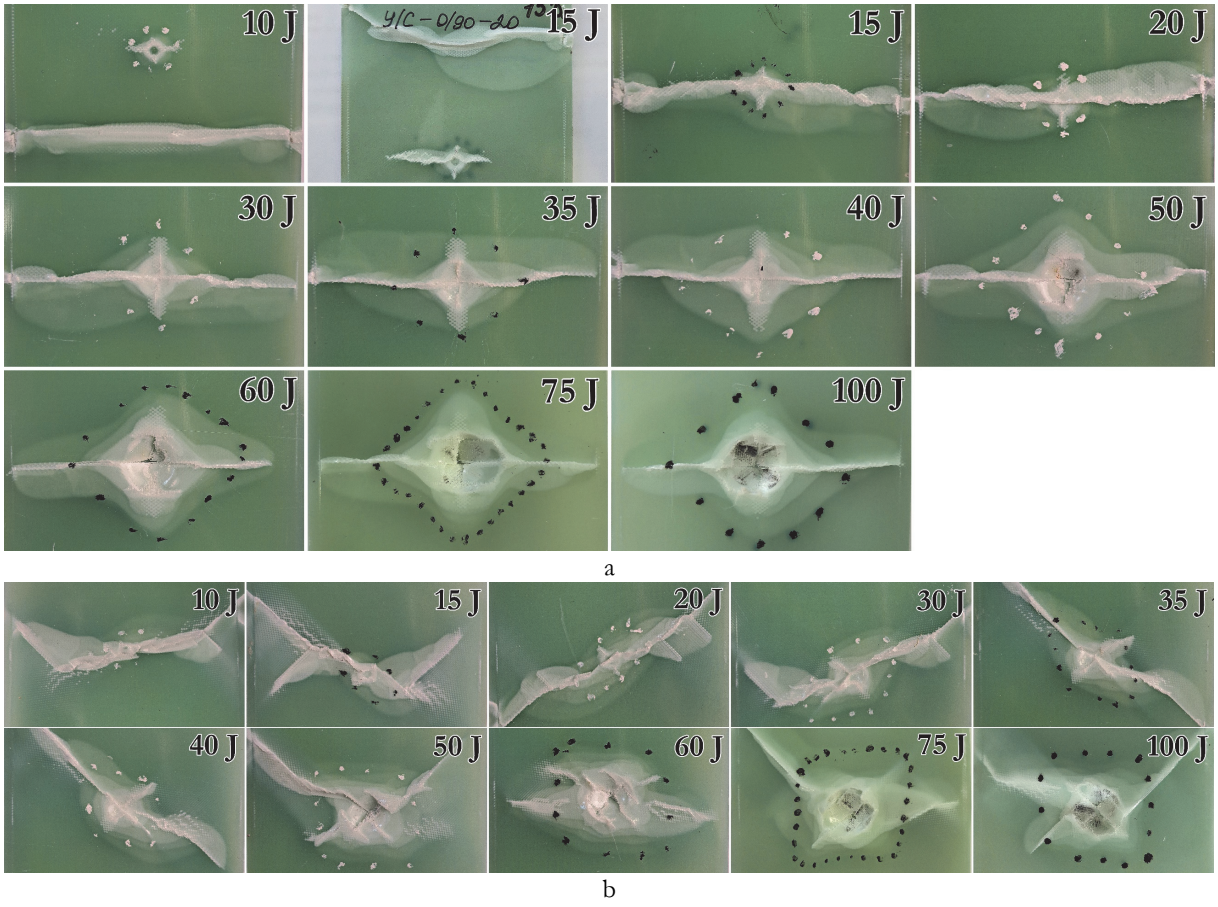

Figure 8: Images of the top side of the specimens with the reinforcement schemes $[0/90]_n$ (a) and $[\pm 45]_n$ (b) after compression

Consideration of some options for functions that meet the above-mentioned requirements.

1. Piecewise-defined function with a power function (C model). This model, previously discussed in [22], is a modification of the Caprino G. [23] model, considering the possibility of the existence of a lower threshold value for the composite's strength:

$$K_F = \frac{F^{CAI}}{F_0^{CAI}} = \begin{cases} 1, E_{imp} \le E_t; \\ \left(1 - \frac{F^{CAI}}{F_{crit}^{CAI}}\right)\left(\frac{E_t}{E_{imp}}\right)^{\kappa} + \frac{F^{CAI}}{F_{crit}^{CAI}}, E_{imp} > E_t. \end{cases} \quad (1)$$

Here $E_t > 0$ is the threshold value of the impact energy, upon reaching which the strength of the composite does not change; $\kappa > 0$ is the shape parameter of the approximating power function. Thus, the model contains three parameters – E_t, $\kappa > 0$, F_{crit}^{CAI}. The disadvantage of the model is a critical point at $E_{imp} = E_t$.

2. Piecewise-defined function with the exponential function (K model). This model is based on the model proposed by Koo J.M. et al [24] and has the form:

$$K_F = \frac{F^{CAI}}{F_0^{CAI}} = \begin{cases} 1, E_{imp} \le E_t; \\ \left(1 - \frac{F^{CAI}}{F_{crit}^{CAI}}\right)\beta^{\left(\frac{E_{imp}}{E_t}-1\right)} + \frac{F^{CAI}}{F_{crit}^{CAI}}, E_{imp} > E_t. \end{cases} \quad (2)$$

Here $E_t > 0$ is the threshold value of the impact energy, upon reaching which the strength of the composite does not change; $\beta > 0$ is the shape parameter of the approximating exponential function. Thus, the model contains three parameters – E_t, β, F_{crit}^{CAI}. The disadvantage of the model is also the critical point at $E_{imp} = E_t$.

3. The model proposed in this paper is based on the use of the arctangent function (AT model). The expression for approximating of the experimental data will be as follows:

$$K_F = \frac{1 + \frac{2}{\pi} a\tan\left(\frac{E_i - E_{imp}}{\lambda}\right)}{1 + \frac{2}{\pi} a\tan\left(\frac{E_i}{\lambda}\right)}\left(1 - \frac{F^{CAI}}{F_{crit}^{CAI}}\right) + \frac{F^{CAI}}{F_{crit}^{CAI}}, \quad (3)$$

where E_i is a coefficient determining the horizontal shift of the arctangent graph (it can be shown that it corresponds to the impact energy at which the curvature of the graph changes, the rate of strength reduction, with an increase in the impact energy, is maximum); $\lambda > 0$ is the scale parameter of the approximating function. Thus, the model also contains three parameters – E_i, λ, F_{crit}^{CAI}. The derivative of the proposed function is continuous, therefore, capable of reflecting smooth processes of damage accumulation. However, the proposed function has a drawback – its derivative is symmetric relative to the straight line $E_{imp} = E_i$, which may not correspond to the experimental data. In order to improve the predictability of this model and to account possible symmetry distortion, the scale parameter can be given as a function of the impact energy, i.e. $\lambda(E_{imp}) \neq const$, but this will require the introduction of additional parameters, which will increase the number of necessary required experiments.

The proposed models were applied for describing the above-mentioned experimental data. Model parameters were determined numerically. The results of parameters determination and coefficients of determination are given in Tab. 4. Graphs of approximation of experimental data are shown in Fig. 9.

Model	F_{crit}^{CAI}, MPa	Parameter 2, J	Parameter 3	R^2
		$[0/90]_n$		
C	89.39	E_t = 18.95	κ = 1.692	0.975
K	96.04	E_t = 18.41	a = 0.271	0.977
AT	95.25	E_i = 29.19	λ = 6.551	0.967
		$[\pm 45]_n$		
C	0.00	E_t = 13.26	κ = 0.154	0.876
K	89.09	E_t = 10.33	a = 0.803	0.881
AT	90.50	E_i = 33.13	λ = 25.088	0.873

Table 4: Results of experimental data approximation

All three models were found to be highly descriptive for approximation of experimental data on the decrease in composite's residual strength after impact: the coefficient of determination exceeded 0.96, with the reinforcement scheme $[0/90]_n$, and 0.87, with the laying scheme $[\pm 45]_n$. At the same time, it should be noted that the model based on the use of the power function led to a zero critical value of the residual strength for the composite $[\pm 45]_n$, which does not correlate with the idea

of the existence of minimum bearing capacity after impact. Also, this model predicts an underestimated value F_{crit}^{CAI} for the composite $[0/90]_n$ in comparison with other models.

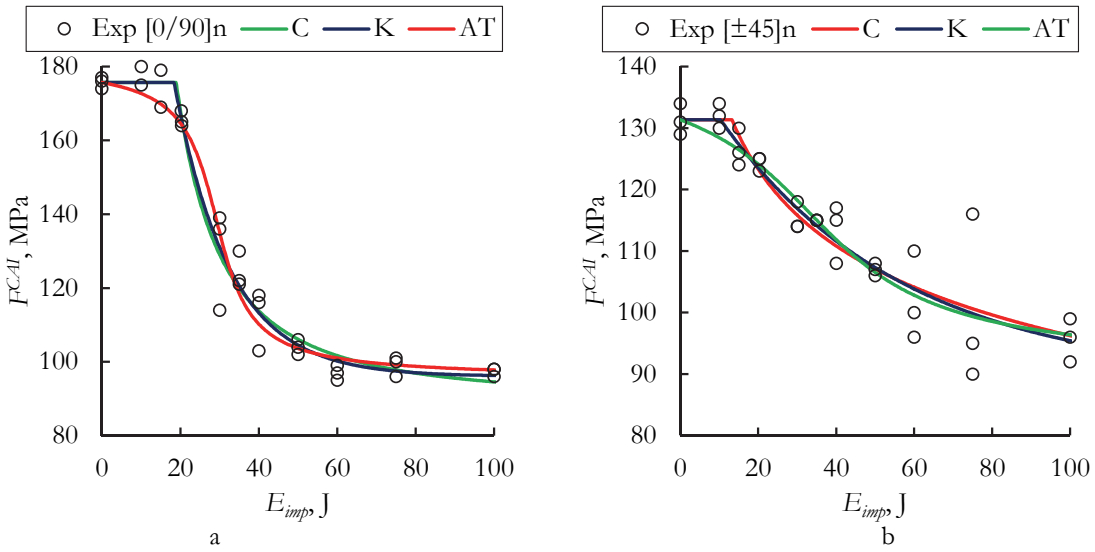

Figure 9: Results of approximation of experimental data for composites with the reinforcement schemes $[0/90]_n$ (a) and $[\pm45]_n$ (b)

The following approach was used to determine the stage boundaries on the impact sensitivity diagrams. The first threshold E_{st1}, corresponding to the end of insensitivity area, for models C and K is introduced explicitly and is equal to the value of the parameter E_t. For the AT model, this threshold is proposed to be determined at the point where the $K_F = 0.95$ value is reached, i.e. a slight decrease in strength by 5 % occurs. The second threshold E_{st2}, corresponding to the transition from the second stage to the third, for all models is introduced as a point, at which the value of K_F is 0.05 higher than the minimum value of the relative bearing capacity of the $F_{crit}^{CAI} / F_0^{CAI}$.

Fig. 10 shows impact sensitivity diagrams with stage boundaries determined in accordance with the proposed approach. Values of impact sensitivity thresholds are given in Tab. 5. The results demonstrate that for the $[0/90]_n$ reinforcement scheme all models predict almost the same threshold value $E_{st1} \approx 18$–19 J. However, for the $[\pm45]_n$ reinforcement scheme, the arctangent-based model results in a slightly overestimated value $E_{st1} \approx 19$ J in comparison with other models, for which $E_{st1} \approx 10$–13 J. Nevertheless, the obtained values are in good agreement with the results of the analysis of the correspondence between the residual strength of the plates and their fractures.

Model	$[0/90]_n$		$[\pm45]_n$	
	E_{st1}	E_{st2}	E_{st1}	E_{st2}
C	18.95	73.17	13.26	3786260356
K	18.41	49.53	10.33	98.11
AT	18.25	49.02	18.71	92.30

Table 5: Threshold values of impact sensitivity

For composite $[0/90]_n$, models K and AT predict close values of $E_{st2} \approx 50$ J – energy, corresponding to breakthrough of the specimen; using model C leads to a significant overestimation of this threshold. It can be concluded that for cross-ply composite, when deformed along the direction of fibers, a breakthrough leads to a decrease in bearing capacity up to almost minimum value. For a composite with a reinforcement scheme $[\pm45]_n$, the use of model C leads to achievement of a high value E_{st2}, more than 1000 J, while models K and AT determine the value of $E_{st2} \approx 92$–98 J, which approximately corresponds to reaching the largest delamination area. A breakthrough in this case does not lead to the achievement of the minimum bearing capacity, which is explained by other mechanisms of damage to the structure during impact and subsequent compression.

Based on the results obtained, it can be concluded that the use of models, based on the exponential function (K model) and the arctangent function (AT model), is more preferable for analyzing the impact sensitivity of GFRP under deformation at different angles to the direction of the fibers, even if in-plane shear is realized. In general, it can be concluded that it is advisable to use the considered models to predict the residual properties of composite plates after impact.

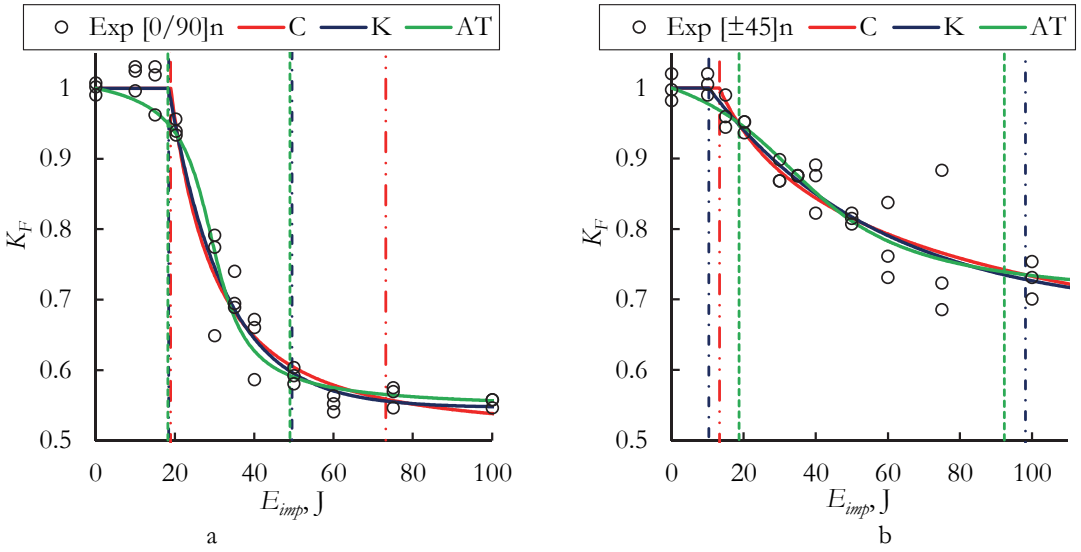

Figure 10: Impact sensitivity diagrams for GFRP $[0/90]_n$ (a) and $[\pm45]_n$ (b)

Conclusions

Based on the results of the study of the influence of preliminary impacts with various energies on the glass fiber reinforced polymer composite's residual strength under compression, the following conclusions were made:

1. There is a qualitative change in the specimen response to the impact (according to the dependence of the load on time and on displacement). In the impact energy range of 10–20 J, pronounced stages of linear and nonlinear load growth and smooth unloading are observed; in the range of 30–50 J, a sharp drop in load is noted after reaching the peak; in the range of 60–100 J, there is a repeated increase in load after reaching the minimum point. These patterns are explained by the various damaging mechanisms, which were also noted as a result of visual inspection of the specimens.
2. There is a quantitative change in the peak load, absorbed energy, and maximum displacement during the impact. The breakthrough energy of the considered GFRP is about 50 J, which is confirmed by the absorbed energy dependence on the impact energy. For specimens with reinforcement scheme $[\pm45]_n$, the peak loads occurring during impact were 8–22% higher than for specimens with stacking sequence $[0/90]_n$, that is explained by the fact that the total length of the fibers, providing primary resistance to the impactor, differs for the two reinforcement schemes.
3. The impact sensitivity diagrams (dependence of the residual strength on the impact energy) constructed for fiberglass laminates with reinforcement schemes $[0/90]_n$ and $[\pm45]_n$ have three characteristic stages: insensitivity to impact, rapid reduction in strength, and reaching of minimum bearing capacity. These stages correlate with various responses of the material to the impact.
4. The considered GFRP has anisotropy in terms of sensitivity to low-velocity transverse impact: reduction in strength of the material with the reinforcement scheme $[0/90]_n$ is about 45%, while for the scheme $[\pm45]_n$ the reduction is about 25%.
5. There is a strong negative linear correlation (the correlation coefficient is below –0.9) between the experimental data on residual strength and delamination area for the examined fiberglass laminate. The possibility of the evaluation of the residual strength after impact based on ultrasonic testing of damaged areas is concluded.
6. Requirements for continuous functions that can be used to approximate experimental impact sensitivity diagrams are defined. In accordance to that, a new model based on the use of the arctangent function has been developed, tested, and compared to models proposed by Caprino G. and Koo J.M. All three models show high descriptive capability: the coefficient of determination exceeded 0.96 for the reinforcement scheme $[0/90]_n$ and 0.87 for the scheme $[\pm45]_n$.
7. A novel approach is proposed for the determination of impact sensitivity thresholds, based on the use of mathematical models. The Koo model and the new model are more suitable for predicting the thresholds. The results demonstrate that

for the $[0/90]_n$ reinforcement scheme, the first threshold value is in the range of 18–19 J and the second threshold value is close to 50 J. For the $[\pm 45]_n$ reinforcement scheme, the first threshold value is in the range of 10–19 J, the second threshold value is in the range of 92–98 J, which approximately corresponds to reaching the largest delamination area.
Further studies will be dedicated to the development of the proposed approach and mathematical models for predicting the residual mechanical characteristics of various polymer composites, such as multilayer panels, 2D and 3D-woven composites, etc. Moreover, it is planned to investigate the influence of the preliminary impact on the fatigue life of composite structures.

ACKNOWLEDGEMENTS

This research was funded by Ministry of science and higher education of the Russian Federation (Project no. FSNM-2024-0013).

REFERENCES

[1] Sun, X.C. and Hallett, S.R. (2018). Failure mechanisms and damage evolution of laminated composites under compression after impact (CAI): Experimental and numerical study, Compos. Part A-Appl. S., 104, pp. 41–59. DOI: https://doi.org/10.1016/j.compositesa.2017.10.026.
[2] Patel, M., Patel, S., Ahmad, S. (2023). Blast analysis of efficient honeycomb sandwich structures with CFRP/Steel FML skins, Int. J. Impact Eng., 178, 104609. DOI: https://doi.org/10.1016/j.ijimpeng.2023.104609.
[3] Zhang, N., Zhou, G., Guo, X., Xuan, S., Wei, D., Wang, X. and Cai, D. (2023). High-velocity impact damage and compression after impact behavior of carbon fiber composite laminates: Experimental study, Int. J. Impact Eng., 181, 104749. DOI: https://doi.org/10.1016/j.ijimpeng.2023.104749.
[4] Zhu, X., Chen, W., Liu, L., Xu, K., Luo, G. and Zhao, Z. (2023). Experimental investigation on high-velocity impact damage and compression after impact behavior of 2D and 3D textile composites, Compos. Struct., 303, 116256. DOI: https://doi.org/10.1016/j.compstruct.2022.116256.
[5] Ge, X., Zhang, P., Zhao, F., Liu, M., Liu, J. and Cheng, Y. (2022). Experimental and numerical investigations on the dynamic response of woven carbon fiber reinforced thick composite laminates under low-velocity impact, Compos. Struct., 279, 114792. DOI: https://doi.org/10.1016/j.compstruct.2021.114792.
[6] Sadighi, M. and Alderliesten, R. (2022). Impact fatigue, multiple and repeated low-velocity impacts on FRP composites: A review, Compos. Struct., 297, 116962. DOI: https://doi.org/10.1016/j.compstruct.2022.115962.
[7] Sapozhnikov, S.B. and Dubovikov, E.A. (2025). The assessment of the severity of local impact on a pro-bionic composite lattice shell by the use of fiber-optic sensors, Fracture and Structural Integrity, 73, pp. 1–11. DOI: https://doi.org/10.3221/IGF-ESIS.73.01.
[8] Naya, F., Pernas-Sánchez, J., Fernández, C., Zumel, P., Droździel-Jurkiewicz, M. and Bieniaś, J. (2024). Experimental study of the importance of fiber breakage on the strength of thermoplastic matrix composites subjected to compression after impact, Compos. Struct., 342, 118238. DOI: https://doi.org/10.1016/j.compstruct.2024.118238.
[9] Qiang, X., Wang, T., Xue, H., Ding, J. and Deng, C. (2024). Study on Low-Velocity Impact and Residual Compressive Mechanical Properties of Carbon Fiber–Epoxy Resin Composites, Materials, 17(15), 3766. DOI: https://doi.org/10.3390/ma17153766.
[10] Staroverov, O.A., Strungar, E.M. and Wildemann, V.E. (2021). Evaluation of the survivability of CFRP honeycomb-cored panels in compression after impact tests, Frattura ed Integrità Strutturale, 56, pp. 1–11. DOI: https://doi.org/10.3221/IGF-ESIS.56.01.
[11] Zhang, C. and Tan, K.T. (2020). Low-velocity impact response and compression after impact behavior of tubular composite sandwich structures, Compos. Part B-Eng., 193, 108026. DOI: https://doi.org/10.1016/j.compositesb.2020.108026.
[12] Yuanjian, T. and Isaac, D. H. (2008). Combined impact and fatigue of glass fiber reinforced composites, Compos. Part B-Eng., 39(3), pp. 505–512. DOI: https://doi.org/10.1016/j.compositesb.2007.03.005.
[13] Mouhoubi, S. and Azouaoui, K. (2019). Residual properties of composite plates subjected to impact fatigue, J. Compos. Mater., 53(6), pp. 799–817. DOI: https://doi.org/10.1177/0021998318791324.
[14] Mirbagheri, M., Rahmani, O. and Mirbagheri, Y. (2022). Estimation of residual tensile strength of composite laminate after low-velocity impact using visually inspection, Eng. Fail. Anal., 131, 105989.

DOI: https://doi.org/10.1016/j.engfailanal.2021.105898.
[15] Staroverov, O.A., Wildemann, V.E., Mugatarov, A.I., Strungar, E.M. and Chebotareva, E.A. (2024). Critical States of Laminated Polymer Composite under Quasi-Static Deformation after Preliminary Low-Velocity Impact Loads, Mech. Solids, 59(5), pp. 3244–3253. DOI: https://doi.org/10.1134/S0025654424606116.
[16] Wan, Y., Wang, L., Liu, Y. and Wu, Y. (2024). Experimental investigation on the low-velocity impact response and the residual strength of CFRP tubes, Polym. Compos., 45(10), pp. 8677–8693. DOI: https://doi.org/10.1002/pc.28368.
[17] Kudryavtsev, O.A., Ignatova, A.V. and Olivenko, N.A. (2021). The Influence of Thickness on Residual Flexural Strength of Composite with Low-Velocity Impact Damages: Experimental Study, PNRPU Mechanics Bulletin, 3, pp. 6–11. DOI: https://doi.org/10.15593/perm.mech/2021.3.01.
[18] Staroverov, O.A., Mugatarov, A.I. and Chebotareva, E.A. (2023). Studying the Regularities of Mechanical Behavior of Fiber Reinforced Plastic Composites under Preliminary Impact and Subsequent Quasistatic and Cyclic Loads, Russian Aeronautics, 66(4), pp. 652–662. DOI: https://doi.org/10.3103/S1068799823040037.
[19] Lin, S., Ranatunga, V. and Waas, A.M. (2022). Experimental study on the panel size effects of the Low-Velocity Impact (LVI) and Compression After Impact (CAI) of laminated composites, Part I: LVI, Compos. Struct., 296, 115822. DOI: https://doi.org/10.1016/j.compstruct.2022.115822.
[20] Lin, S., Ranatunga, V. and Waas, A.M. (2022). Experimental study on the panel size effects of the low velocity impact (LVI) and compression after impact (CAI) of laminated composites, part II: CAI, Compos. Struct., 295, 115824. DOI: https://doi.org/10.1016/j.compstruct.2022.115824.
[21] Patel, M., Sonkar, L., Patel, S. (2025). Assessment of Ply Stacking Sequence Effect on Damage Behavior of CFRP Composite Laminate Under Low-Velocity Impacts, Adv. Mater. Sci. Eng., 2025(1), 4349535. DOI: https://doi.org/10.1155/amse/4349535.
[22] Staroverov, O.A., Strungar, E.M., Mugatarov, A.I. and Dubrovskaya, M.A. (2024). Residual Strength and Fatigue life of Woven Composite under Compression after Impact Loading, PNRPU Mechanics Bulletin, 5, pp. 106–119, DOI: https://doi.org/10.15593/perm.mech/2024.5.09.
[23] Caprino, G. (1984). Residual strength prediction of impacted CFRP laminates, J. Compos. Mater., 18(6), pp. 508–518. DOI: https://doi.org/10.1177/002199838401800601.
[24] Koo, J.M., Choi, J.H. and Seok, C.S. (2013). Prediction of residual strength of CFRP after impact, Compos. Part B-Eng., 54, pp. 28–33. DOI: https://doi.org/10.1016/j.compositesb.2013.04.020.
[25] Strungar, E., Lobanov, D., Mugatarov, A. and Chebotareva, E. (2024). Deformation processes of polymer composites with stress concentrators under different reinforcement schemes, J. Reinf. Plast. Comp., DOI: https://doi.org/10.1177/07316844241281780.